applied sciences

MDPI

Article

Climate Impact Reduction Potentials of Synthetic Kerosene and Green Hydrogen Powered Mid-Range Aircraft Concepts

Daniel Silberhorn [1,*,†], Katrin Dahlmann [2,†], Alexander Görtz [3,†], Florian Linke [4,†], Jan Zanger [5,†], Bastian Rauch [5,†], Torsten Methling [5,†], Corina Janzer [5,†] and Johannes Hartmann [1,†]

1 Deutsches Zentrum für Luft- und Raumfahrt, Institut für Systemarchitekturen in der Luftfahrt, 21129 Hamburg, Germany; johannes.hartmann@dlr.de
2 Deutsches Zentrum für Luft- und Raumfahrt, Institut für Physik der Atmosphäre, 82234 Oberpfaffenhofen, Germany; katrin.dahlmann@dlr.de
3 Deutsches Zentrum für Luft- und Raumfahrt, Institut für Antriebstechnik, 51147 Cologne, Germany; alexander.goertz@dlr.de
4 Deutsches Zentrum für Luft- und Raumfahrt, Lufttransportsysteme, 21079 Hamburg, Germany; florian.linke@dlr.de
5 Deutsches Zentrum für Luft- und Raumfahrt, Institut für Verbrennungstechnik, 70569 Stuttgart, Germany; jan.zanger@dlr.de (J.Z.); bastian.rauch@dlr.de (B.R.); torsten.methling@dlr.de (T.M.); corina.janzer@dlr.de (C.J.)
* Correspondence: daniel.silberhorn@dlr.de
† These authors contributed equally to this work.

Abstract: One of aviation's major challenges for the upcoming decades is the reduction in its climate impact. As synthetic kerosene and green hydrogen are two promising candidates, their potentials in decreasing the climate impact is investigated for the mid-range segment. Evolutionary advancements for 2040 are applied, first with an conventional and second with an advanced low-NO_x and low-soot combustion chamber. Experts and methods from all relevant disciplines are involved, starting from combustion, turbofan engine, overall aircraft design, fleet level, and climate impact assessment, allowing a sophisticated and holistic evaluation. The main takeaway is that both energy carriers have the potential to strongly reduce the fleet level climate impact by more than 75% compared with the reference. Applying a flight-level constraint of 290 and a cruise Mach number of 0.75, causing 5% higher average Direct Operating Costs (DOC), the reduction is even more than 85%. The main levers to achieve this are the advanced combustion chamber, an efficient contrail avoidance strategy, in this case a pure flight-level constraint, and the use of CO_2 neutral energy carrier, in a descending priority order. Although vehicle efficiency gains only lead to rather low impact reduction, they are very important to compensate the increased costs of synthetic fuels or green hydrogen.

Keywords: aviation; climate impact assessment; liquid hydrogen; synthetic fuel

Citation: Silberhorn, D.; Dahlmann, K.; Görtz, A.; Linke, F.; Zanger, J.; Rauch, B.; Methling, T.; Janzer, C.; Hartmann, J. Climate Impact Reduction Potentials of Synthetic Kerosene and Green Hydrogen Powered Mid-Range Aircraft Concepts. *Appl. Sci.* **2022**, *12*, 5950. https://doi.org/10.3390/app12125950

Academic Editor: Georgios Karavalakis

Received: 28 April 2022
Accepted: 8 June 2022
Published: 11 June 2022

1. Introduction

The continuously growing demand for air transport must be aligned with the increasingly urgent need of society to significantly reduce the environmental impact of aviation and to bring its climate impact in line with the Paris climate targets, as well as to bring air quality and noise emission in line with local regulations. Several aircraft concepts, technology bricks, and operation strategies are currently under investigation in a vast variety of research projects. The aim of the present study is to contribute to the goal of identifying solutions with drastically reduced climate impact. The focus is on a comparative assessment of two green energy carrier options for a mid-range aircraft segment. More specifically, a synthetic kerosene version based on green hydrogen and direct air capture (DAC) is compared against liquid hydrogen (LH2) in a gas turbine propulsion architecture.

The order numbers for the A321neo indicate a strong future market potential for the mid-range segment, which is applied as a representative product scenario. To tackle the

multidisciplinary aircraft architecture and integration with the necessary level of detail, experts from all relevant fields participate in the study. That workflow includes detailed combustion chamber computations, complex engine performance modelling, a comprehensive overall aircraft design synthesis, and a surrogate climate chemistry response model applied on a defined global fleet scenario and route network, see Figure 1. The following CO_2 and non-CO_2 effects are taken into considerations as major climate impact contributors from aviation:

- Direct CO_2 effects;
- Total NO_x impact;
- Water vapour;
- Contrail induced cloudiness (CiC).

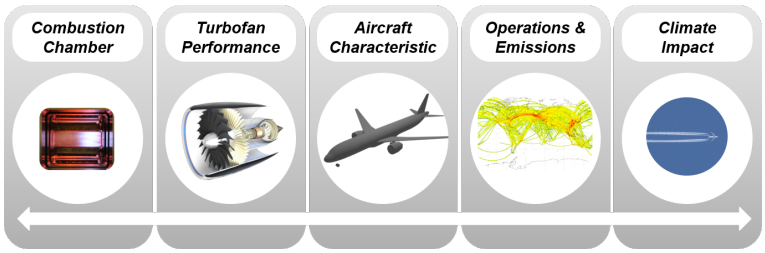

Figure 1. Overview of involved expertises.

CO_2 contributions can potentially be reduced by changing the energy carrier to renewable produced variants such as green hydrogen and synthetic fuel. Furthermore, a low-NO_x and low-soot combustion chamber is utilized to strongly reduce the NO_x effects. In addition to the change of the energy carrier and updated low-NO_x technology options, the aircraft design was optimized for maximum contrail effect reductions by varying maximum operational altitudes and cruise Mach numbers. As flying lower and slower also comes with increased costs, the direct operating costs are calculated to balance the economic effects of the aforementioned concepts. Besides this specific climate impact reducing measures, the aircraft utilizes evolutionary efficiency improving technologies such as high bypass ratio geared turbofan engines and carbon fibre reinforced polymers (CFRP) as wing and empennage structural material.

The investigated concepts are listed below:

- D261: Reference based on B767-300.
- D261+: Baseline for entry into service (EIS) 2040 with evolutionary advancements and fossil kerosene.
- D261+DropIn: Similar to D261+, but designed and operated with 50% drop-in blend.
- D261+SAF: Similar to D261+, but designed and operated with 100% synthetic kerosene. An altitude constraint, cruise Mach number trade, is conducted.
- D261+H2: Same technological assumptions as D261+ but designed and operated with 100% green liquid hydrogen. An altitude constraint—cruise Mach number trade is conducted.

All future concepts are designed with a conventional and advanced low-NO_x/low-soot combustion technology. Furthermore, only the in-flight climate impact is considered, as the operation of commercial aircraft accounts for by far the biggest part of its life cycle. As it is assumed that the drop-in blend and the synthetic kerosene are produced with renewable carbon sources such as direct air capturing (DAC), the in-flight CO_2 emissions of these fuel portions do not cause any climate impact.

2. Materials and Methods

All disciplines involved are separately described within this section to provide an impression of the various methods and their fidelity levels. Due to the integrative character, more detailed descriptions of the methodologies can be found in several citations of each field.

2.1. Energy Carrier Characteristics

The energy carrier characteristics are applied throughout the whole evaluation chain. An overview of the key parameters is listed in Table 1. The data for hydrocarbon fuels are taken from DLR SimFuel property database, which consists of several thousand units of fossil kerosene and several hundred Sustainable Aviation Fuels. All fuels were chosen to be representative of a fuel from their respective category. Furthermore, the Jet A-1 (ECLIF Ref 3) and the drop-in blend (ECLIF SAF2) were both used during flight campaigns measuring fuel impact on emissions and contrail formation [1]. The drop-in fuel is a 30% blend of HEFA (Hydroprocessed Esters and Fatty Acids) and Jet A-1 applies to ASTM D7566 fuel specification, whereas the power to liquid (PtL) synthetic fuel contains no aromatics and is thus outside current fuel specifications (starting in March 2021, different options for 100% Sustainable Aviation Fuel (SAF) specification are being discussed [2]).

It can be seen in Table 1 that the lower heating value (LHV) increases from Jet A-1 to PtL, whereas the density decreases. This is mainly due to reduced (blend) or zero amount of aromatics in the fuel (PtL), which in turn increases hydrogen and decreases carbon content. This is also visualized by the two emission indexes (EI). The density of the LH2 fuel is valid for a pressure of 0.12 MPa and temperature of 20.96 K. However, the open-source library Cantera [3] is applied for the specific fuel characteristics of LH2 at each flight condition. Both the drop-in blend as well as the PtL synthetic kerosene are utilizing direct air capturing (DAC) as the carbon source as well as green hydrogen. Furthermore, the energy carrier production process is assumed to be carbon neutral.

Table 1. Key characteristics and emission properties of applied energy carriers.

	Unit	Jet A-1	Drop-In	PtL	LH2
LHV	MJ/kg	43.138	43.639	44.184	119.96
Density	kg/m^3	814.7	777.2	752.7	70.2
EI CO_2	kg_{CO2}/kg_{Fuel}	3.164	3.132	3.101	0.0
EI H_2O	kg_{H2O}/kg_{Fuel}	1.220	1.297	1.374	8.937

2.2. Combustion Chamber

The kerosene powered concepts for 2040 are assessed with two combustion chamber options.

2.2.1. Conventional Combustion

To predict the NO_x emissions of the conventional combustion chamber at flight conditions, a methodology presented in [4] is used. This methodology enables the calculation of emissions at altitude conditions based on ground level emission data. The reference emissions are published by the ICAO [5]. To use the p3-T3-method, reference functions of the emission index (EI), which is the mass flow of emissions per fuel flow, the pressure, and the fuel-to-air ratio (FAR) have to be created:

$$EI_{NO_x} = f(T_3) \qquad p_{3,Ref} = f(T_3) \qquad FAR_{Ref} = f(T_3) \tag{1}$$

The index 3 stands for the combustion chamber entry. To receive information regarding T_3, the reference engine model of the CF6 is used and the reference functions are approximated with quadratic functions. The equation below is used to determine emissions at every point in the flight envelope in terms of the emission index.

$$EI_{NO_x} = EI_{NO_{x,Ref}} \cdot \left(\frac{p_3}{p_{3,Ref}}\right)^{\alpha} \cdot \left(\frac{FAR}{FAR_{3,Ref}}\right)^{\beta} \tag{2}$$

Appropriate values for α and β can be found in [6].

These emissions are appropriate for the original CF6 engine, but not for the engines used for the D261+ concept in this paper. As the same p3-T3-method is applied for the entry into service (EIS) 2040 case, the reference functions have to be adapted. This adaptation is accomplished by the DLR/Stöppler method [6–8].

The DLR/Stöppler method is based on a simplified description of the actual physical and chemical processes for the nitrogen oxide formation. Therefore, many influences on this formation can be considered and analysed as follows:

$$\frac{EI_{NO_x}}{EI_{NO_{x,Ref}}} = \frac{1+\frac{1}{FAR}}{1+\frac{1}{FAR_{Ref}}} \cdot \frac{\dot{m}_{Air,Ref}}{\dot{m}_{Air}} \cdot \left(\frac{p_3}{p_{3,Ref}} \cdot \frac{T_{PZ,Ref}}{T_{PZ}}\right)^c \cdot e^{\frac{E}{R}\cdot\left(\frac{1}{T_{FL}}-\frac{1}{T_{FL,Ref}}\right)} \quad (3)$$

Similar to the p3-T3-method, the reference functions are approximated using combustion chamber entry temperature and values from the CF6 engine. Further constants are $E = -312$ kJ/Mol and the universal gas constant $R = 8.3143$ J/(Mol K). The temperature in the primary zone T_{PZ} can be calculated with the entry temperature T_3 and the equilibrium temperature T_Φ as follows:

$$T_{PZ} = \frac{T_3 + T_\Phi}{2} \quad (4)$$

Furthermore, the flame temperature T_{FL} is calculated with the equilibrium temperature T_Φ, the stoichiometry temperature $T_{\Phi=1}$, and the weighting factor r_{FL}:

$$T_{FL} = r_{FL} \cdot T_\Phi + (1 - r_{FL}) \cdot T_{\Phi=1} \quad (5)$$

The constant values for c (Equation (3)) and r_{FL} (Equation (5)) are selected so that the emission indices EI_{NO_x} and $EI_{NO_{x,Ref}}$ in Equation (3) match at 30% and 100% ground thrust.

The emissions adapted by the DLR/Stöppler method are still the emissions for the ground level case. For the D261+, the adapted ground emissions are used to determine emissions at flight conditions with the previously presented p3-T3-method.

2.2.2. Advanced Combustion

In order to achieve a significant reduction in exhaust gas emissions in the future forecast, the FLOX (Flameless Oxidation) based combustion concept was chosen for the gas turbine. Here, the DLR institute of combustion technology has a deep expertise in the development, system integration, and operating behaviour in FLOX-based gas turbine combustion systems for stationary power supply [9–13]. The FLOX-based technology was chosen as it showed in many projects [14–17] advantages in NO_x emission levels, robustness towards thermo-acoustics, lean blow-off limits as well as fuel flexibility compared to swirl-stabilized concepts. Even though this technology is not yet present in aircraft gas turbines, recent projects aim to transfer this technology into the aircraft application to utilize these benefits [18].

As much more experience and experimental data of the FLOX-based technology is available in a can combustor setup, a cannular combustion chamber concept was chosen for the simulations to improve the confidence in the results. A predesign of the setup was completed resulting in a setup with three separate cans comprising of a single staged FLOX-based combustor with 16 individual air and fuel nozzles each. The layout of one of the cans is shown in Figure 2. The power density of each can was chosen as 0.5 kW/(m^3·Pa) with a liner volume of approximately 5.6 L. The concept of a single stage combustor simplifies the numeric modelling and validation by experimental data. Numerical analyses of the combustion in the complete given gas turbine operating range have shown that a single FLOX-based stage is feasible to stabilize the combustion in the operational envelope; however, at ignition and gas turbine ramp-up, a second stabilizing stage would be needed. These operating conditions are neglected in the following analysis.

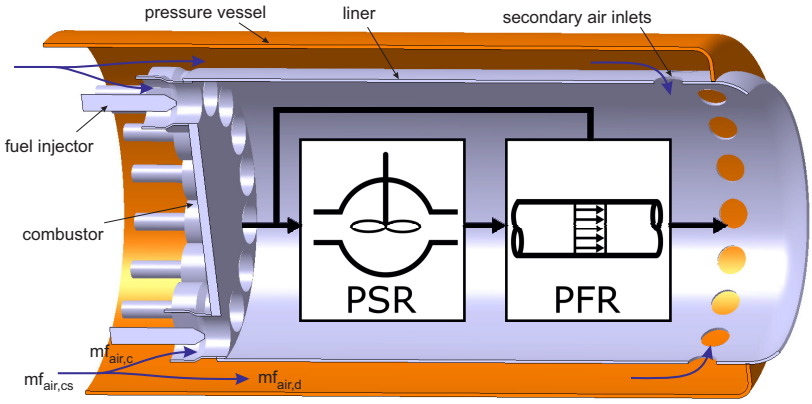

Figure 2. Generic setup of each of the FLOX-based can combustors, together with the schematic of reactor network.

A reactor network validated to several FLOX-based combustion experiments is used as the numeric model of the combustion chamber [11]. This model takes pressure, temperature, and mass flow of both fuel and air as input parameters from the turbo fan engine performance simulation, and it delivers exhaust gas emission indices (NO_x, CO, CO_2, and H_2O) to the combustion chamber. Soot emission calculations are not included in the model, but these are approximated in a postprocessing step (see Section 2.2.3). Additionally, the load point depending total pressure loss of the combustion chamber is derived from scaled experimental results and delivered to the further tool chain. The fuel composition is a further boundary condition which also defines the selected kinetic reaction model. The split between primary ($\dot{m}_{air,c}$) and secondary air ($\dot{m}_{air,d}$) is a free model parameter and serves as an optimization variable regarding emission levels and combustion stability. In the following sections the air split S_D is defined as:

$$S_D = \frac{\dot{m}_{air,c}}{\dot{m}_{air,c} + \dot{m}_{air,d}} \cdot 100\% \quad (6)$$

The reactor network is based on a previously applied design [11] and consists of two homogeneous reactors, as delineated in Figure 2. The main recirculation zone of the FLOX based combustor is modelled with a perfectly stirred reactor (PSR). The burnout zone is represented by a plug flow reactor (PFR). In the FLOX based combustion process, gas from the burnout zone is partially recirculated to the main combustion zone. To model this recirculation, half of the mass flow from the PFR is diverted to the inflow of the PSR (Figure 2). This mass flow is diverted at the distance of 90% of the total length of the PFR. The size of the recirculation zone is dependent on various boundary conditions. The influence of the mass flow, temperature, and pressure on the size of the recirculation zone was correlated with results from prior investigation on FLOX based combustion systems [11,19,20] in terms of the volume fraction V_{psr}/V_{tot}, which is the volume if the perfectly stirred reactor divided by the total volume. The results for this correlation are shown in Figure 3.

The residence time within the PSR and PFR are then defined by the mass flow and the volume of the reactors. Due to the heat loss, the exhaust gas temperature was estimated to be 2.5% below the adiabatic flame temperature. The heat loss in the reactors was set accordingly to achieve this user given exhaust gas temperature decrease in the model.

The reactor network approach including the correlation for the recirculation zone was validated by comparing numerical results from the reactor network and corresponding experimental data of different FLOX-based combustors. The good agreement between the model and experiments is exemplary shown for on of these cases in Figure 4. In these graphs the comparison of the reactor network and the single burner experiments of a 15 kW FLOX-based combustor is shown for carbon monoxide (CO) and nitrogen oxide (NO_x)

emissions as a function of global air-fuel equivalence ratio λ. For a better comparison, both emissions are shown normalized to 15 Vol-% O_2 as common reference in gas turbine combustion. The comparison was conducted for a 15 kW FLOX-based combustor with 6 nozzles, as well as for a 333 kW FLOX-based combustor with 20 nozzles utilizing different gaseous fuels. In these simulations, the used parameters of the network were kept constant. Only the residence time inside the reactors were adjusted corresponding to the geometry of the combustors. The very good agreements of simulation and experiment for both studied combustors provide confidence to the authors that the reactor network is scalable to higher fuel power as used in the recent study.

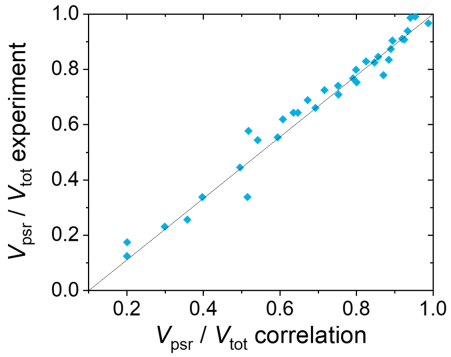

Figure 3. Correlation results for the estimation of the recirculation zone of the reactor network.

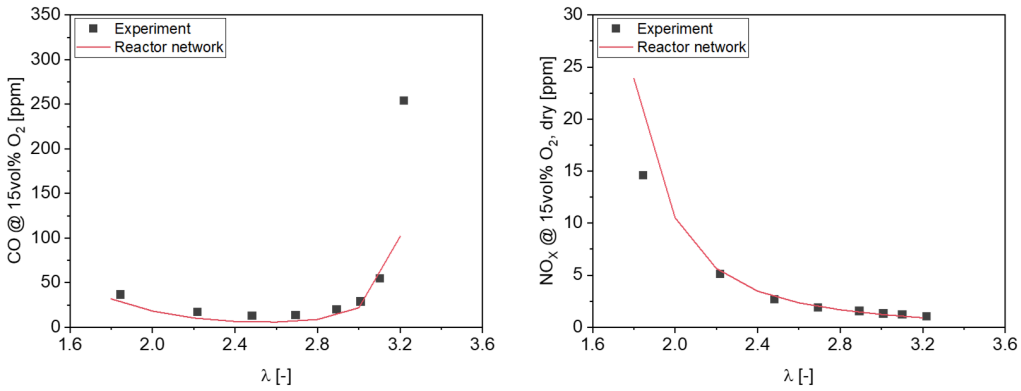

Figure 4. Validation of the reactor network with experimental data from a FLOX based natural gas combustor [20] at 69% of maximum thermal power.

To model kerosene, the Jet A-1 surrogate E2-Ref3 was selected from prior work [21]. The Jet A-1 surrogate was modelled with the chemical kinetic mechanism DLR Concise [22]. The chemical kinetic mechanism is designed to model jet fuel combustion under gas turbine conditions. The mechanism is validated for numerous jet fuel components from the chemical classes of n-, iso-, and cyclo-alkanes, as well as aromatics. Additionally, the mechanism is validated for various real fuel surrogates, including the Jet A-1 surrogate E2-Ref3. To investigate the NO formation, the mechanism was extended with the NO_x submodel from Glarborg et al. [23].

2.2.3. Soot Emissions

Despite the sophisticated NO_x prediction, the soot emissions for the advanced combustion technology case had to be derived from reference data by experts involved in this study. Data from the ICAO emission databank [24] show that today's LEAP-X and GEnx engines already reduce the soot emissions by several orders of magnitude. However, these data are based on the Landing and Take-Off (LTO) cycle which leads to uncertainties in this assumption. Nevertheless, as below 10% soot emissions of the reference the climate impact assessment methodology, described in Section 2.6, assumes the surrounding particles to be

dominating, the expectable soot emission reduction seems to exceed this threshold. Despite the soot emission reduction by combustion chamber technologies, the fuel type (and its associated fuel hydrogen content) plays an important role, too. As seen in Table 2, the 30% blend drop-in and PtL kerosene reduce the soot number to 69% and 38%, respectively, whereas for hydrogen it even vanishes. These reductions are assumed to be independent of the combustion technology and are based on finding from the ECLIF in-flight measurement campaigns [1].

Table 2. Relative soot number reduction potentials.

	Unit	Jet A-1	Drop-In	PtL	LH2
Conventional Combustion	%	100	69	38	0
Low NO_x/Soot Combustion	%	<10	<10	<10	0

2.3. Turbofan Engine Performance

The virtual engine platform Gas Turbine Laboratory (GTlab) [25,26], which is developed at the Institute of Propulsion Technology of the German Aerospace Center (DLR), is used to design the engines. The DLR Performance Program (DLRp2) [27] is linked to the performance interface of GTlab and is used for the thermodynamic cycle evaluation. The following engine design uses a General Electric CF6 Engine as reference and is newly designed for the year entry into service (EIS) 2040. This engine model is a two-spool geared and unmixed turbofan. The fan, booster and high-pressure-compressor are driven by a two staged high-pressure turbine and a low-pressure turbine, which is assumed to be uncooled. The corresponding engine architecture is shown in the performance model Figure 5. The numbers represent the common naming of stations inside turbofan engines [28].

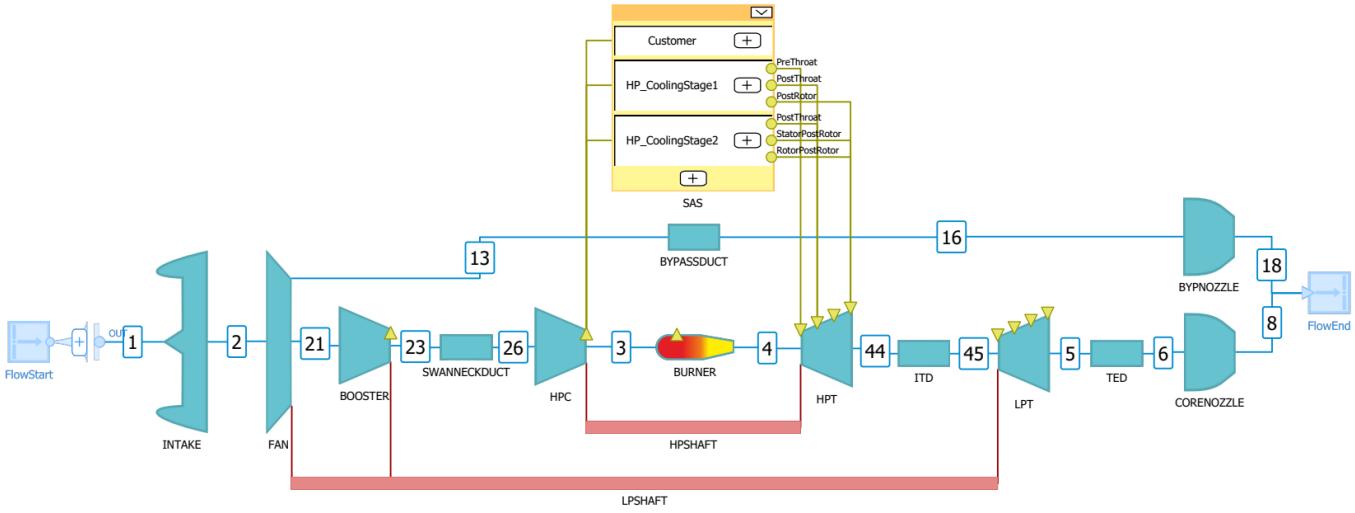

Figure 5. Schematic view of the engine architecture in the virtual engine platform Gas Turbine Laboratory (GTlab) [25,26].

Overall, there have been two engines designed. The first covers all three types of kerosene, and the second is for the hydrogen fuelled engine. Both engines were separately designed for cruise. The influence of the turbocomponents size, regarding the corrected mass flow rate, on the efficiency is based on correlations from [29]. These correlations also include the loss in efficiency due to the use of cooling air in the turbines. The fan bypass ratio is determined by matching the nozzle speed ratio with the ideal nozzle speed ratio, and while the bypass ratio increases the fan pressure ratio has to be reduced [30,31]. Both engines have the same fan diameter, and the intake mass flow rate is matched to achieve the required thrust. To determine the low-pressure shaft speed, the turbine loading parameter AN^2 at the outlet of the low-pressure turbine is used [29]. This parameter characterizes the

stress of the turbine rotor blade and is typically the highest at either take-off or top of climb. For the purpose of a high engine efficiency, the overall pressure ratio and the turbine entry temperature are essential. In this case, the maximum overall pressure ratio is defined by the compressor outlet temperature. Therefore a maximum for both values has been set [32]. This limit will not be reached in the design point cruise but will be reached at take-off conditions. By limiting the maximum temperatures within the whole operating range, these temperatures are indirectly defined for the design point. The engines were designed for cruise conditions as this is the point in which the aircraft will be operation most of the time and therefore provide a minimal overall fuel consumption. Nevertheless, other important off-design points, such as take-off, top of climb, and end of field, have also been considered to examine thermal and mechanical loads. As the thrust requirements of the hydrogen engine differ from the requirements for the kerosene engine, it is not possible to use the same method for determining the temperature limits for the hydrogen engine. The temperatures at turbine entry and compressor outlet will be set to the same value for both engines for cruise conditions. This provides the opportunity to perform an appropriate comparison between both fuels. Furthermore, the hydrogen is stored in liquid form but has to be vaporized for the combustion. The heat required for this process is taken from the exhaust flow after the low-pressure turbine. The additional mass for evaporation is not considered, whereas the thermodynamic effects at engine level are included.

2.4. Aircraft Design and Operating Costs

The overall aircraft design is conducted by integrating several disciplinary tools into a workflow which is built in RCE [33]. The data schema CPACS [34,35] is applied to allow a seamless communication between the disciplines. The core component is the handbook based tool openAD [36]. A more detailed description of the workflow can be found in [37]. The results of the high fidelity turbofan engine performance simulations, together with the emission characteristics, are integrated in engine performance decks which can be interpreted by the mission performance tool. This assures a clean interface and sophisticated results of the aircraft's behaviour at any possible flight state in the missions. As Mach number and maximum altitude trades are conducted, the methodologies have to be capable to include the necessary dependencies with the correct sensitivities. Consequently, a minimum set of input parameters has to be used which incorporates the low-speed aerodynamics and performance calculations.

For calibration and validation purposes, the Boeing 767-300 [38] is recalculated and the top level aircraft requirements (TLAR) are derived, see Table 3. The B767 is used as a reference, as it's entire family, B767-200, B767-300, and B767-400, perfectly matches the promising future market segment of 200–300 passengers with its typical two class layouts leading to 216 to 296 available seats [38]. The design range of 3900 NM also fits between the short-range single aisle aircraft with design ranges of less than 3000 NM and modern long-range aircraft such as the Airbus A350 and the Boeing B787 with design ranges of more than 8000 NM. Furthermore, the twin aisle layout is used to cover the upper end in terms of range and available seats of the mid-range market segment, whereas the lower end could potentially be covered by a single aisle concept similar to an Airbus A321neo. The focus of this study is on the upper end of the mid-range market segment as this also allows a potential substitution of some long-range flights. Additionally, the twin aisle concept reduces the boarding and de-boarding times compared to a long single-aisle layout which is in most cases at the critical path of turnaround schedules.

The main challenge of liquid hydrogen powered aircraft is the storage and distribution. This is why more advanced methods are applied, including a dynamical thermodynamic calculation of the tank behaviour along the trajectories. A detailed description of LH2 tank design methods can be found in [39]. Correlations by Brewer [40] are applied to estimate the mass of the storage subsystems as well as the distribution lines.

Table 3. Top Level Aircraft Requirements.

	Unit	Value
Design Range	NM	3900
Design PAX (two class)	-	261
Design Payload	kg	26,100
Cruise Mach number	-	0.8
TOFL (ISA SL)	m	2400
Approach Speed (MLM)	kt	140
Wing Span Limit	m	52

Even though this study focuses on the climate impact reduction potentials of synthetic kerosene and green liquid hydrogen, operating costs are calculated only to capture the impact of forcing the aircraft to fly lower and slower. The operating costs are calculated by applying the methods described in [41,42] which is the extended TU Berlin method [43,44]. The direct operating costs consist of air-traffic-control, ground handling and landing fees, maintenance costs, crew costs, energy costs, and capital expenditures (CAPEX). The recurring costs (RC), which are typically the main portion of the capital expenditures (CAPEX), are calculated by [45] where the production costs of each aircraft part is calculated separately. This method is extended by a LH2 tank price correlation extracted from [46]. For the unconstrained LH2 concept D261+H2, a price of 6.2 million USD is calculated for the two storage tanks and subsystems. The energy carrier production costs are taken from [42] which provides data for comparable boundary conditions. For power to liquid kerosene, 42.8 USD/GJ, and for LH2 34.8 USD/GJ is applied, both based on averaged electricity costs of 12.5 USD/GJ. This are the important assumptions concerning the difference between synthetic kerosene and liquid hydrogen. For further details of this method, see [41,43,44].

2.5. Global Fleet Analysis and Operations

The non-CO_2 climate effects depend on the locus of the emissions, i.e., geographic longitude/latitude and altitude. Hence, in order to determine the different climate impact reduction potentials, the operations of the aircraft propulsion concepts are modelled within a global fleet. In a first step, a potential global route network, which could be serviced by the aircraft, is derived. As a basis, global fleet forecast data from the project WeCare [47] are used, which is available as flight schedule data per aircraft seat category for the years 2015 to 2050 in 5-year increments. The global route network in terms of flown distance (km) with longitudinal, latitudinal, and altitude distribution is shown in Figure 6.

With a passenger capacity of 261 seats (see Table 3), the new mid-range aircraft is assumed to be a potential candidate for the 200 to 300 seats market. Similar to the methodology applied in [48], the above mentioned flight schedule data for the respective seat categories are filtered for those routes, which can be operated by a mid-range aircraft designed for a 3900 NM range. Then, flight missions are computed in increments of 100 NM to determine a set of aircraft trajectories with the aircraft state variables, including flight distance, pressure altitude, and fuel and emission flows as a function of time. Based on that, a database of reduced emission profiles is generated by using the aircraft state at the phase transitions as support points for characterizing the profile. Standard profiles with a typical speed schedule are assumed and, where appropriate, step climbs are conducted to optimize the cruise altitude according to maximum specific range. We then apply the GRIDLAB tool [49,50] to map the aircraft mission-level performance to the global fleet. For every route (including flight frequency) in the flight schedule, the appropriate reduced emission profile is obtained from the database, adjusted to match the exact length of the flight, and projected onto the great circle connection between the origin and destination airports. The emission distributions of the individual flights are rasterized and finally superposed to three-dimensional inventories of CO_2, H_2O, and NO_x emissions, as well as of flown distances. Those constitute the basis for the climate impact assessment.

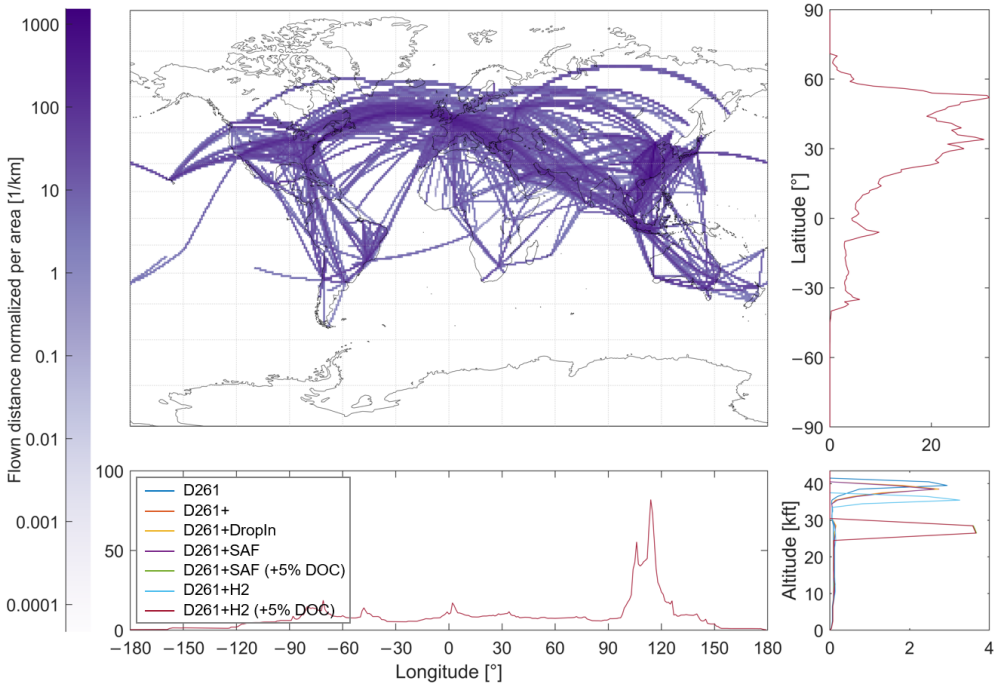

Figure 6. Global distribution of flown distances covered by the underlying route network.

2.6. Climate Impact

To calculate the climate impact of different aircraft configurations the non-linear climate-chemistry response model, AirClim [51,52] is applied. AirClim is a surrogate model which combines air traffic emissions, calculated, e.g., by GRIDLAB, with pre calculated atmospheric impact data. For the pre calculated data, climate–chemistry simulations are performed, with normalised emissions in idealised emission regions. For the impact of NO_x emissions on the O_3 and CH_4 concentration, and for the impact of H_2O emissions, the complex climate–chemistry model E39C/A [53] was used. For the climate impact of CiC (contrail induced cloudiness) simulations with the ECHAM4-CCMod model [54] were analysed. The climate impact of CO_2 is independent of the emission location due the long lifetime. Therefore, a green function based on [55] is used for the climate impact of CO_2. AirClim calculates the concentration change, RF (Radiative Forcing) and near surface temperature change of the individual species accounting for their different life time and dependency of the emission location. The AirClim model presented in [52] was generated for conventional fuel consumption. For alternative fuels such as sustainable aviation fuel (SAF) or hydrogen, the number of emitted soot particles is reduced, which influence contrail properties and RF. To account for this, a relation between relative change in particle emission and resulting change in RF is applied, which is received from simulations from [56]:

$$\Delta RF^{CiC} = \frac{arctan(1.9\Delta pn^{0.740})}{arctan(1.9)} \tag{7}$$

where Δpn is the relative change in particle number emissions (dimensionless value between 0 and 1) [57]. Using liquid hydrogen instead of conventional kerosene changes both the particle emission and the probability of contrail formation. The Schmidt–Appleman Criterion (SAC) suggests whether contrails form and persist. This depends both on the ambient temperature and humidity on the slope of the G-factor [58]:

$$G^* = \frac{EI_{H_2O}}{(1-\eta)LHV} \tag{8}$$

where EI_{H_2O} is the emission index of water vapour, η is the overall propulsion efficiency, and LHV is the lower heat value of the fuel. If the slope increases, the probability of contrail formation increases. Additionally, η influence the contrail coverage by [47]

$$F(LH2) = \frac{\eta}{\eta_{conventional}}. \quad (9)$$

For assessing the climate impact of the different aircraft configurations, the average near surface temperature change over 100 years (Average Temperature Response, ATR100) is analysed. An entry into service of 2040 and a life time of 32 years is assumed. As background atmosphere, the RCP4.5 scenario is applied, which is a middle of the road scenario [59].

3. Results

3.1. NO_x Reduction Potential

While the concepts with conventional combustion chambers show no advancements in NO_x and soot emissions, the advanced combustion technology shows significant reduction. At global fleet level, the NO_x emissions could be reduced by 91% for the kerosene case and by 99.8% for the hydrogen concept compared with the reference D261. This strong reduction is mostly due to three features. Firstly, the combustion is operated at very lean conditions with the help of a wider stable operating range of the FLOX-based combustion technology compared to conventional swirl-stabilized combustion. Secondly, the authors assume that fully prevaporized fuel injection can be handled at an entry into service of 2040. Therefore, near stochiometric conditions around spray droplets are not present in the combustion, which helps to decrease the NO_x emissions. Thirdly, due to the high momentum jets, the FLOX-based combustion achieves more homogeneous temperature profiles, reducing high temperature peaks and strong NO_x sources, respectively.

Assumptions on the combustion's lean blow off (LBO) limits at different input fuels were derived from atmospheric combustion experiments. Measurements of different FLOX-based combustors utilizing various gaseous fuels have shown that the global air-fuel equivalence ratio λ at LBO is $\lambda_{LBO} \geq 2.8$ for relevant air preheat temperatures [9,19,60]. Therefore, the λ_{LBO} was chosen at 2.6 using prevaporized Jet A-1. Using pure hydrogen, the stable operating range is much wider. Recent unpublished experiments of a FLOX-based combustor using pure hydrogen have shown that the air–fuel equivalence ratio at LBO is >5. In this study, the λ_{LBO} was conservatively chosen to 3.6 using pure hydrogen.

The air split S_D is a free parameter in the reactor network. In order to select an optimized air split for the Jet A-1 and the hydrogen fuel case, characteristic turbo fan load points were chosen for a trade-off study. As described in Section 2.2.2 the combustion chamber inlet conditions were taken from the turbo fan performance simulations (see Section 2.3). For the trade-off study, five characteristic load points were chosen from the fuel specific performance decks: take-off, end of field, second segment, top of climb, and mid cruise. For these load points NO_x emissions were traded off against combustion stability. As a marker for combustion stability, the calculated CO emissions were used. As a result of this trade-off study, the air split S_d was fixed for the detailed emission study. On the basis of this study, the air split at hydrogen fuelled combustion was set to 87% and to 65% for Jet A-1 furled combustion.

In the detailed emission calculations, 86 load points along the mission flight trajectory were selected from each fuel specific engine performance map (hydrogen and Jet A-1). The reactor network simulations were carried out for these load points at a fixed air split. For each of these load points, the emissions (NO_x, CO, H_2O, and CO_2) were simulated for both hydrogen and Jet A-1. The results were provided as a combustion emission map to the climate impact analysis.

With the reactor network, the effect of air–fuel equivalence ratio in the combustor λ_c on the total NO_x formation was investigated for the two fuel scenarios. Figure 7 shows an increase in the NO_x emission indices EI with decreasing λ_c for both fuel options for a

constant flight Mach number of 0.8. This trend is related to the formation of thermal NO, which is pronounced by increasing adiabatic flame temperatures with the decrease in λ_c. For identical λ_c, the adiabatic flame temperature of hydrogen flames is higher than the ones for Jet A-1. Nevertheless, due to the reactivity of hydrogen, hydrogen combustion allows a stable combustion at leaner mixing conditions compared to Jet A-1. Therefore, the formation of NO_x is similar, or can even be reduced by substituting kerosene with hydrogen, as shown in Figure 7. This is achieved by choosing leaner conditions at the primary combustion zone in the hydrogen case and shifting the air split S_d towards more secondary air. This choice was made well inside the stable combustion regime. Figure 7 also shows a weak dependency of the flight level on the NO_x formation. The increase in the NO_x formation is also caused by increasing combustor inlet temperatures for increased engine ratings, leading to slightly higher thermal NO productions.

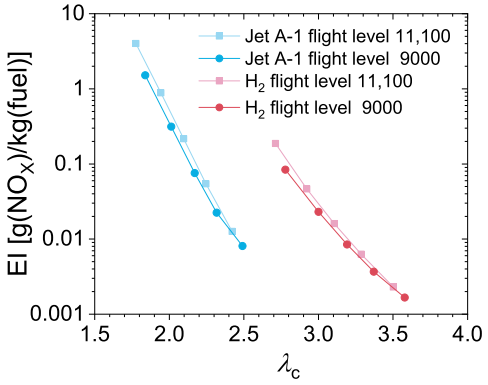

Figure 7. Reactor network results of NO_x emission index dependency on with the variation of λ_c.

3.2. Turbofan Engine Performance

Usually, an important value to evaluate flight gas turbines is the fuel consumption, or more precisely the thrust specific fuel consumption. By comparing two fuels with different lower heating values and densities, this approach is no longer reasonable, as the fuel mass flow will be different. Alternatively, another value can be considered for a similar validity, which is the thrust specific energy consumption (TSEC). The TSEC describes the amount of energy added to achieve the required thrust. In this study, the TSEC decreases by 6.7% when using hydrogen instead of kerosene. Using hydrogen as fuel results in a higher amount of water in the core flow. This increased water ratio is responsible for a higher energy density due to the higher heat capacity of water or in this case steam. As the temperature at the combustor outlet is the same but the heat capacity is increased, the turbines can provide more power with the same amount of mass flow. By setting the fan diameter to a defined value and using the methods mentioned above, this results in a higher bypass ratio for the hydrogen fuelled engine. This effect is also responsible for the decreased energy needed to provide the thrust. Looking at the required thrust levels in Table 4 for the operating points cruise and take-off, it can be seen that the needed thrust at cruise conditions is rather similar for both engines. On the other hand, the needed thrust at take-off differs on a lager scale. In particular, the ratio between cruise thrust to take-off thrust is different between concepts. This means that the hydrogen engine has to be loaded much less at take-off conditions compared to cruise conditions. At this point, it is important to notice the boundary conditions regarding the temperature limits for the hydrogen case, mentioned in the methods. Using the same turbine entry temperature at the design point results in a lower temperature level at take-off conditions due to the relative lower required thrust. The hydrogen engine is capable of providing the take-off thrust at lower temperatures.

Table 4. Turbofan Performance Characteristics.

	Unit	D261+SAF	D261+H2
BPR	-	16.2	17.3
OPR	-	51.0	50.9
TET max	K	1850	1731
TET mid. cruise	K	1613	1613
Thrust mid. cruise	kN	29.3	31.7
Thrust SL static	kN	189.5	168.6
TSEC	W/N	579	540

3.3. Aircraft Design

The results at aircraft level are presented in the following section. In total, there are five major concepts. First, the reference aircraft D261 based on the Boeing 767-300 with conventional combustion chambers and fossil Jet A-1. Second, there is the new design D261+, which is an evolutionary advancement of the D261 based on the entry into service (EIS) of 2040. This incorporates an advanced high-bypass-ratio turbofan engine and high aspect ratio carbon fibre reinforced wings. Furthermore, this concept and all further hydrocarbon fuel based ones are evaluated twice, first equipped with an conventional combustion chamber and second with new low-NO_x and low-soot technology. Figure 8 shows the increased span and the reduced wing and horizontal tailplane area.

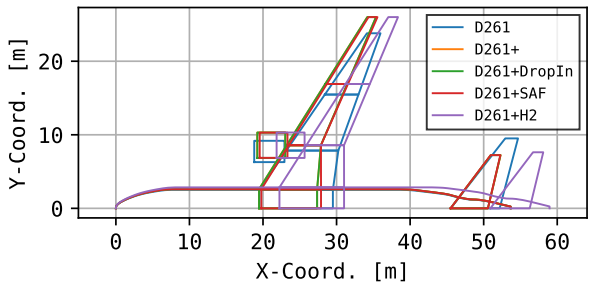

Figure 8. Generic top view of all concepts.

The next two concepts D261+DropIn and D261+SAF incorporate the same technology bricks but are operated and designed for the drop-in capable fuel and the synthetic one, respectively. The differences in mass, geometry, and performance are rather small. Last, the liquid hydrogen powered aircraft D261+H2 is designed with the same technology assumptions. The big LH2 tanks are integrated in front and behind the cabin, see Figure 9. The access of the pilots to the cabin is not considered, as this would penalize the aircraft's performance and there is no official regulation. However, the drawback is the additional lavatory and galley inside the cockpit, which adds weight and needs to be serviced. Furthermore, two additional exits or one exit and one top hatch are needed, as the first two doors of the cabin, which are considered to be in the flight crew area, are not accessible, see CS 25.807 [61]. However, having a long tunnel between cockpit and cabin should result in the same problem. To better maintain a reasonable fines ratio of the fuselage, the diameter has been increased to accommodate an eight-abreast cabin arrangement. The insulation architecture of the cryogenic tanks is foam with a carbon fibre load carrying inner wall and an kevlar outer wall for protection. This reduces the maximum tank volume and the total vented gaseous hydrogen. The maximum operational pressure is set to 0.25 MPa and additional 5% inner tank volume is required for safety aspects. The delivery of the fuel to the consumer is conducted in the liquid state. The high pressure pumps and the heat exchanger for evaporation are installed near the engines. The total mass of the tank structure, delivery lines, and tank subsystems is roughly 9 tonnes, which leads to a total gravimetric index of about 50%. In addition, the maximum operating altitude and the cruise Mach number are traded for the D261+SAF and D261+H2 concepts to reduce the climate

impact of the altitude dependent non-CO_2 contributions. The maximum altitude constraint is varied between flight level 290 and 410 whereas the cruise Mach number varies between 0.75 and 0.8. For each of these points, a new design is conducted incorporating new sweep angles and high-lift performance. Figure 8 shows the generic top view of all concepts. All new concepts have an increased wing span of 52 m compared with the reference D261. The fuselage width and length of the LH2 aircraft design is increased due to the integration of the big storage tanks which is also visible in Figure 8.

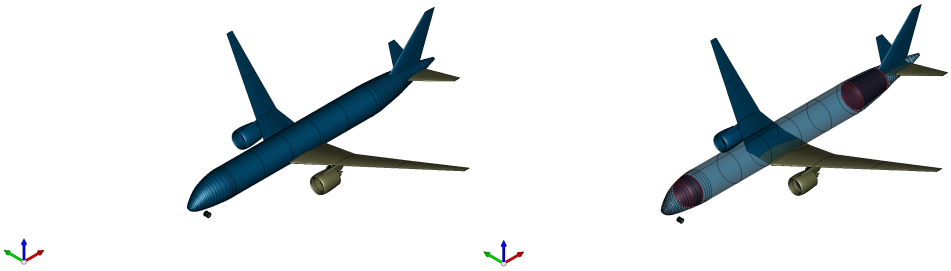

(**a**) (**b**)

Figure 9. Isometric view of 2040 Kerosene D261+SAF (**a**) and LH2 concept D261+H2 (**b**).

The masses of all concepts for the MTOM and maximum payload case are shown in Figure 10. The masses of all new kerosene based concepts are strongly reduced compared to the reference D261. This is due to the new materials and manufacturing methods as well as the increased efficiency and the correlated lower fuel mass and structural snowball effects. Additionally, the maximum payload has been reduced for all new concepts. Interestingly, the MTOM of the D261+H2 decreases whereas the operational empty mass (OEM) increases. Especially the increased maximum landing mass (MLM) and the decreased MTOM explains the relaxed low-speed thrust requirements, as the wing area is sized for MLM conditions. The structural LH2 storage mass as well as the subsystems and delivery lines are accounted as systems which is why this portion strongly increase in Figure 10.

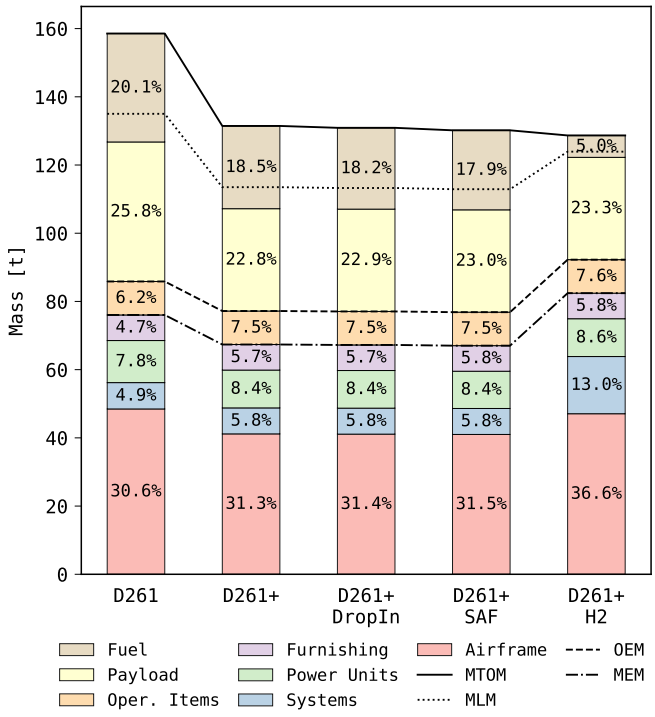

Figure 10. Masses of all concepts for the MTOM with max. payload case.

Table 5 shows several major results at aircraft level. It can be seen that the reference area decreases for the 2040 kerosene concepts and strongly increases again for the LH2 one due to the increased MLM. The thrust loading for take-off and top of climb (TOC) conditions based on an equivalent thrust at sea level (SL) and MTOM shows that the high speed requirements are more sizing for the LH2 concept. That means that the optimal flight altitude is more a trade between power installed and aerodynamic performance, which is why LH2 aircraft concepts tend to fly at slightly lower altitudes than the aerodynamic optimum. Another advantage is that the engine can be down-rated for low speed conditions, which has a positive effect at maintenance and allows shorter take-off field lengths (TOFL). The explained reduced difference between MTOM and MLM is also the reason why the wing loading based on MTOM is lower for the D261+H2 than for the 2040 kerosene concepts. The lift to drag ratio increases for the new 2040 kerosene concepts compared to the reference, mainly due to the increased span and reduced averaged cruise mass, or in other words due to the reduced lift per wing span. The aerodynamic performance decreases again for the D261+H2 due to the wider and longer fuselage to accommodate the LH2 storage tanks. The maximum high lift coefficient C_L is slightly smaller for the D261+H2 as the wider fuselage reduces the useful wing area to install high lift devices. The block energy of the new kerosene based concepts for 2040 decreases by roughly 39%, which mainly results from the increased overall propulsion efficiency. The additional structural mass, together with the reduced aerodynamic efficiency, shown in Table 5 in terms of lift to drag ration, increases the block-energy of the D261+H2. However, the increased engine efficiency of roughly 7%, explained in Section 3.2, dampens these effects, leading to only an additional 3% block-energy at design range and payload compared with the D261+SAF concept. For smaller ranges, this difference increases due to the higher structural mass fraction of the D261+H2. For a 800 nm mission, the difference is already 6%.

Table 5. General aircraft results.

	Unit	D261	D261+	D261+DropIn	D261+SAF	D261+H2
MTOM	kg	158,550	131,455	130,905	130,170	128,670
OEM	kg	85,850	77,190	77,060	76,850	92,245
MLM	kg	135,010	113,500	113,260	112,910	123,915
Ref. Wing Area	m^2	283.3	217.9	217.4	214.3	241.6
Wing Span	m	47.6	52	52	52	52
Thrust loading TO	-	0.291	0.292	0.291	0.289	0.261
Thrust loading TOC	-	0.230	0.263	0.263	0.263	0.270
Wing Loading (MTOM)	kg/m^2	559.7	603.3	602.2	607.4	532.5
Overall Efficiency (FL350)	%	32.4	40.4	40.4	40.4	43.6
LoD mid. Cruise	-	18.3	20.7	20.7	20.7	19.6
CL max. Landing	-	2.23	2.43	2.43	2.43	2.39
Block-Energy (3900 NM)	GJ	1720	1054	1050	1044	1074

The D261+SAF and the D261+H2 concepts are varied in maximum flight level constraints and cruise Mach number. For each flight level, a new concept is designed to meet the same requirements. The following Figures 11–14 show vehicle specific dependencies of the the cruise Mach number and the maximum allowable flight level variation for a representative 1500 NM mission. In general, it can be noted that the lower the flight level constraint for one cruise Mach number, the worse the overall performance. The main reason for this is the overall propulsion performance and the aerodynamic behaviour. The Lift-over-Drag ratio (LoD) decreases with decreasing flight levels as the aircraft is forced to fly at lower than optimal lift coefficients. As the first order effects for the aerodynamic optimum flight level are wing loading and speed, this effect can be mitigated by also reducing the flight level, as seen in Figure 12. The wing loading in cruise can be influenced by the high lift capabilities in landing configuration. For high maximum lift coefficients, the wing can be designed smaller leading to a higher overall wing loading. However, the maximum fuel capacity

for the kerosene concepts has to be considered and becomes limiting for more aggressive high lift coefficients. The overall propulsion efficiency decreases with decreasing flight level constraints as the thrust matching between low speed and high speed requirements is not optimal. The low speed is much more sizeable which leads to an off design operation in cruise. While the engine is operated at about 83% of the maximum thrust at cruise rating for the FL 410 and 0.8 Mach number case, allowing barely the required rate of climb of 300 ft/min, the FL 290 and 0.8 Mach number case is operated at around 54%. However, the turbofan is designed for the flight level 410 and Mach 0.8 case and is scaled for the other concepts with different constraint settings. Therefore, the effects shown in Figure 13 can potentially be weakened. Another promising solution could be to boost the turbofan in low speed conditions and design it especially for the specific cruise requirements. The Block-Energy (BE) is shown in Figure 14. Both concepts show rather similar behaviour. By simply reducing the flight level, the aircraft is forced to fly at non ideal aerodynamic and propulsion conditions leading to strong block energy increases of more than 20%. This can partially be compensated by also reducing the cruise Mach number.

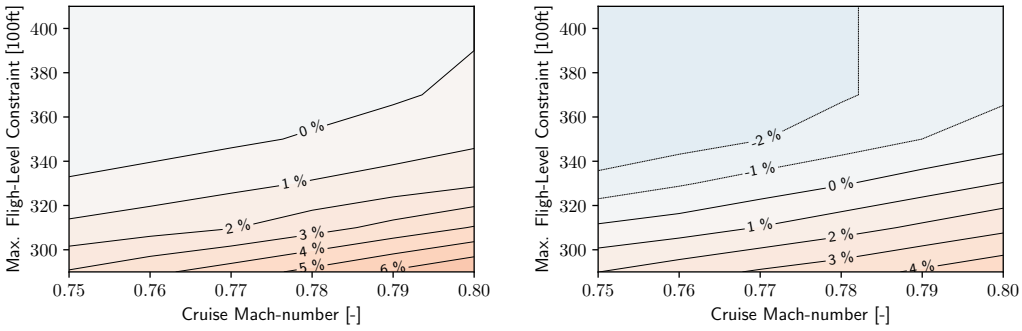

(**a**) (**b**)

Figure 11. MTOM difference for PtL concept D261+SAF (**a**) and LH2 concept D261+H2 (**b**).

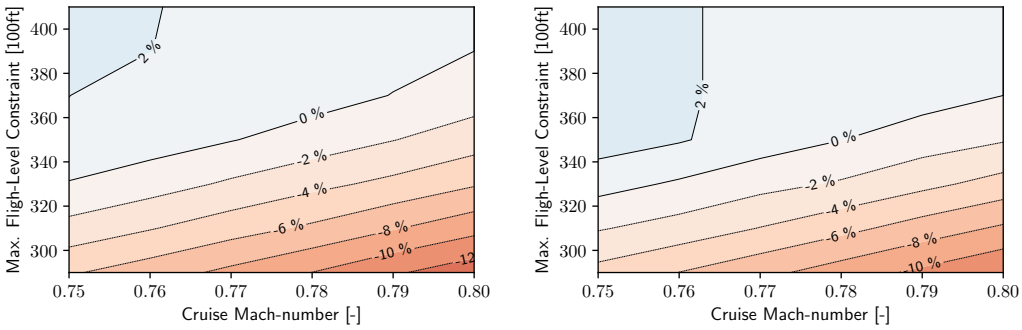

(**a**) (**b**)

Figure 12. LoD difference for PtL concept D261+SAF (**a**) and LH2 concept D261+H2 (**b**).

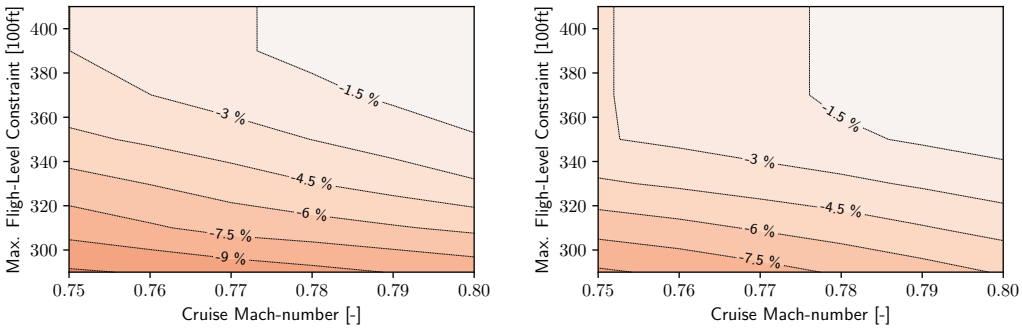

(**a**) (**b**)

Figure 13. Total propulsion efficiency difference in mid-cruise for PtL concept D261+SAF (**a**) and LH2 concept D261+H2 (**b**).

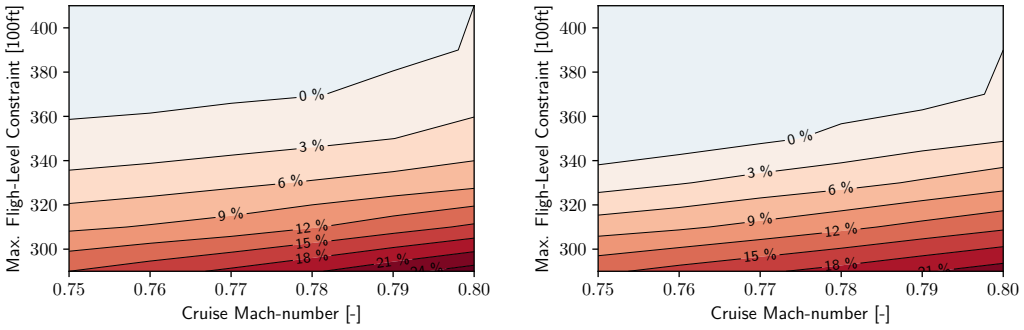

Figure 14. Block-Energy difference for PtL concept D261+SAF (**a**) and LH2 concept D261+H2 (**b**).

3.4. Global Emissions and Climate Impact Results

The overall results in terms of emissions and climate impact of the different concepts evaluated at global fleet level are shown in Figures 15 and 16. Furthermore, the global distribution of emissions is visualized in Appendix A. The grey cells in Figures 15 and 16 indicate the changes per step. The reference aircraft D261 is used to normalize the global emissions and the Average Temperature Response (ATR). The ATR is calculated for a time frame of 100 years and 32 years of operation, starting in 2040. For the D261, the impact of CiC is responsible for 53% and the total NO_x impact, consisting of increased global ozone (O_3) and increased depletion rates of methane (CH_4) for 23%, the carbon dioxide for 19%, and water vapour for 5%. The D261+ with conventional technology advancements for 2040 shows benefits in CO_2 and water vapour which correlates with the improved fuel consumption. However, the increased temperatures in the conventional combustion chamber cause higher NO_x emissions, which compensates the benefit of reduced fuel consumption. Additionally, the contrail impact could potentially increase due to the correlation with the overall propulsion efficiency of the turbofan engines. Nevertheless, this has to be interpreted with care as this correlation is based just on few reference points (see Section 2.6). Despite the strongly reduced fuel consumption, the potential climate impact reduction is not significant and could even be worse, indicated by the uncertainties. For the advanced combustion chamber, the climate impact is reduced by 65%. In addition to the benefits in CO_2 and H_2O, the advanced combustion chamber (low NO_x and low soot) reduces the climate impact of CiC and NO_x due the reduced NO_x and particles emission of 91% and 90%, respectively.

The next two concepts, D261+DropIn and D261+SAF in Figures 15 and 16, have the same technology level as the D261+ but are powered with drop-in capable kerosene, considering today's standards, and with 100% synthetic kerosene produced by PtL. Whereas the redesign has little effect at vehicle performance level, the change in climate impact is much higher. The CO_2 emissions and impact is strongly reduced for the D261+DropIn and vanishes for the D261+SAF. This is due to the assumption of carbon neutral fuel production incorporating Direct Air Capturing (DAC) as carbon source. For the conventional combustion chamber, the contrail impact is lowered due to the reduced soot emissions of the drop-in and PtL fuel, see Table 1. The gradual reduction for the D261+DropIn and D261+SAF with advanced combustion chambers results not from the reduced contrail effect, as the soot emissions are already at the lowest provable level where the particles in the environment are dominating the properties of contrails, but from the CO_2 neutral production with DAC. All concepts described thus far are operated at performance optimized flight levels. The next concept, displayed in Figures 15 and 16, reduces the maximum flight level as well as the cruise Mach number to 290 and 0.75, respectively. This results in 5% higher direct operating costs (DOC) compared to the D261+SAF at optimum flight levels, mainly caused by higher crew costs, capital expenditures, and fuel consumption. As the CO_2 impact is eliminated within this scenario, the reduced aircraft performance is merely visible. However, the altitude reduction strongly affects the non-CO_2 effects, which leads to a reduction of 56% compared to the non restricted case and 69% compared to the

reference scenario with conventional combustion. For the advanced combustion chamber, the reduction compared to the reference reaches 93%.

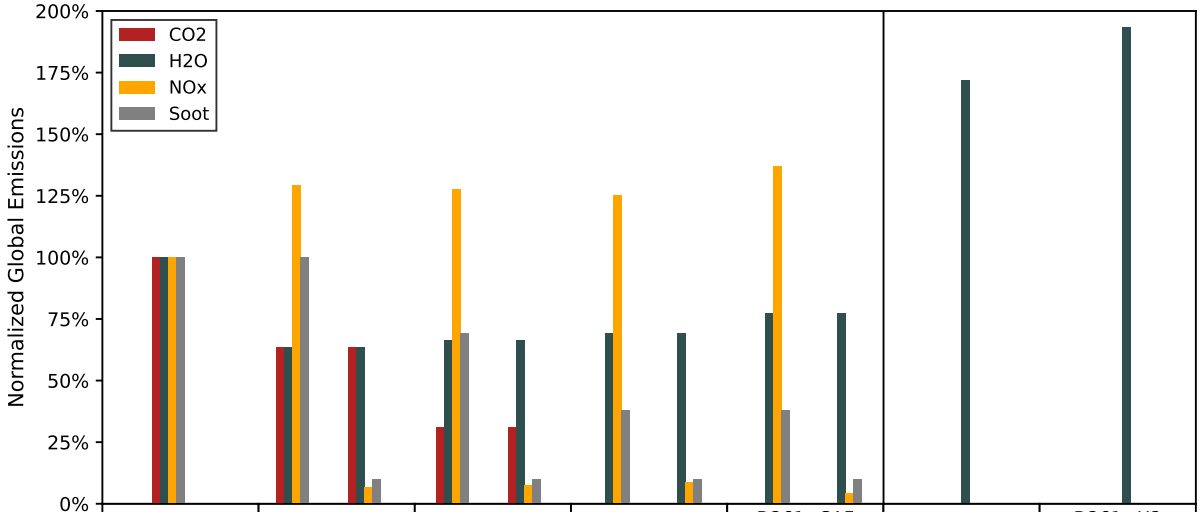

	D261	D261+		D261+DropIn		D261+SAF		D261+SAF +5% DOC		D261+H2	D261+H2 +5% DOC
Energy Carrier	Fossil Kerosene	Fossil Kerosene		Drop-In Fuel		SynFuel		SynFuel		Green LH2	Green LH2
Entry Into Service	1986	2040		2040		2040		2040		2040	2040
Combustion Chamber	Conventional	Conventional	Low NOx Low Soot	Conventional	Low NOx Low Soot	Conventional	Low NOx Low Soot	Conventional	Low NOx Low Soot	Low NOx	Low NOx
Max. Flight-Level	FL 410	FL 410		FL 410		FL 410		FL 290		FL 410	FL 290
Cruise Mach-Number	0.8	0.8		0.8		0.8		0.75		0.8	0.75

Figure 15. Relative global changes in emissions with conventional and advanced low-NO_x and low-soot combustion. The grey cells indicate the changes of the new scenario compared with the preceding neighbour.

The uncertainties of all low NO_x and low soot combustion are rather high, as the effect of reduced soot emissions at contrail impact is not yet understood profoundly. For conventional combustors, a major part of volatile particle (vPM) emissions condenses on non volatile particle (nvPM) emission. This effect and its impact on contrail impact is well understood. In case of a low NO_x and low soot combustor, the level and role of vPM on contrail formation has not been examined and is not clear. This is reflected by an additional uncertainty of the low NO_x and low soot combustor model results in Figure 16.

The last two columns in Figures 15 and 16 are LH2 concepts, the first with no flight level restrictions and the second with the flight level restriction of 290 and a cruise Mach number of 0.75, which causes the same 5% increase in DOC as in the D261+SAF case. The total NO_x emissions and impact vanishes due to the advanced combustion, described in Section 3.1. Due to the strongly increasing water vapour emissions for LH2 concepts, the water vapour climate impact also increases by 40% compared with the unrestricted D261+SAF. However, due to the low overall impact of water vapour, this strong increase merely affects the overall impact. Furthermore, it can almost be eliminated for the restricted D261+H2 case, shown in the last columns of Figure 16. The LH2 contrail uncertainties are relatively high as the reference simulations for the climate impact correlation for LH2 are to few to allow a more specific conclusion. However, this confidence band shows the potential range and allows a first comparison with synthetic kerosene concepts.

Summarized, the unrestricted synthetic kerosene with conventional combustion and LH2 concepts result in a 31% and 75% climate impact reduction compared to the reference, respectively. The flight level restricted concepts achieve a 69% and 85% reduction for the synthetic kerosene with conventional combustion and LH2 scenarios, respectively. The four kerosene concepts for 2040 with advanced combustion show a significant reduction in total NO_x as well as contrail impact. This leads to a reduction of 65% for the D261+ and

77% for the D261+SAF. The flight level restricted scenario even leads to a 93% reduction in the climate impact compared to the reference.

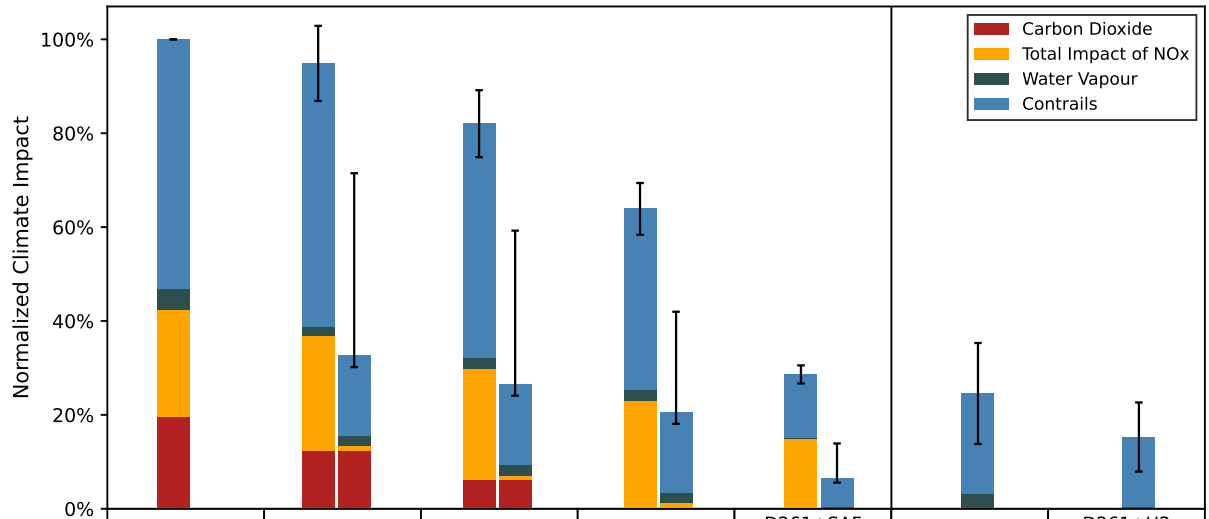

	D261	D261+		D261+DropIn		D261+SAF		D261+SAF +5% DOC		D261+H2	D261+H2 +5% DOC
Energy Carrier	Fossil Kerosene	Fossil Kerosene		Drop-In Fuel		SynFuel		SynFuel		Green LH2	Green LH2
Entry Into Service	1986	2040		2040		2040		2040		2040	2040
Combustion Chamber	Conventional	Conv-entional	Low NOx Low Soot	Conv-entional	Low NOx Low Soot	Conv-entional	Low NOx Low Soot	Conv-entional	Low NOx Low Soot	Low NOx	Low NOx
Max. Flight-Level	FL 410	FL 410		FL 410		FL 410		FL 290		FL 410	FL 290
Cruise Mach-Number	0.8	0.8		0.8		0.8		0.75		0.8	0.75

Figure 16. Relative change in climate impact (ATR100) with conventional and advanced low-NO_x and low-soot combustion. The grey cells indicate the changes of the new scenario compared with the preceding neighbour. The uncertainties are visualized by the black whisker lines.

4. Conclusions

The current study offers potential pathways for significantly reducing the climate impact of future air-vehicle concepts. It also provides the direct comparison of synthetic kerosene and LH2 powered future representative aircraft concepts in terms of climate impact with all relevant disciplines and fidelity levels involved. The main takeaways are listed below:

- The block-energy for the design mission of the liquid hydrogen (LH2) concept is just 3% higher than the synthetic kerosene one. This is due to the increased overall turbofan engine efficiency of about 7% which counteracts the aerodynamic and structural penalties.
- The increased engine efficiency results from the higher water content in the exhaust. This leads to a higher energy density due to the increased heat capacity which results in more powerful turbines for the same mass flow.
- The LH2 concept shows relaxed, low-speed thrust requirements leading to lower turbine entry temperatures at take-off engine rating compared with the kerosene concepts. This is due to the smaller difference between MTOM and MLM which results from the higher energy density of LH2. The wing area and high-lift system is sized for Maximum Landing Mass (MLM) condition leading to lower wing loadings at Maximum Take-Off Mass (MTOM).
- Compared to the reference concept, the advanced combustion technology based on the Flameless Oxidation (FLOX) concept achieves 91% and 99.8% global NO_x emission reduction for kerosene and hydrogen, respectively.
- The biggest lever in climate impact reduction is the advanced low-NO_x and low-soot combustion chamber technology. The difference between the D261+ which is an

evolutionary baseline concept for entry into service (EIS) 2040 and fossil fuel with conventional combustion and the one with advanced combustion chambers (FLOX) is 67%. This reduction is due to the strongly decreased NO_x and particles emission, which causes a reduction in the total NO_x and contrail induced cloudiness (CiC) impact. In other words, the rigorously implementation of advanced low-NO_x and low-soot combustion chamber technology leads to 67% impact reduction.

- The second biggest lever is the implementation of flying in lower altitudes to effectively reduce the non-CO_2 effects. In this study, a pure altitude constraint of flight level 290 and an reduced Mach number of 0.75 is applied leading to significant non-CO_2 impact reductions, but also to 5% higher global fleet level Direct Operating Costs. This impact reduction can potentially be further increased if additional, more precise measures, such as flexible no-fly zones for very sensitive airspaces, are employed.
- The third biggest lever is the use of sustainable energy carriers. Together with the previous two measures and the assumption of green hydrogen and synthetic kerosene with renewable carbon sources, a combined climate impact reduction of 85% and 93% for the LH2 and the synthetic kerosene case can be achieved, respectively. Although the impact in terms of Average Temperature Response (ATR) is only the third biggest, the reduction in CO_2 emissions is very important, on the one hand due to the very long lifetime of CO_2 in the atmosphere, and on the other hand due to the additional fuel consumption for flying in lower altitudes for avoidance of non-CO_2 effects.
- Significant climate impact reductions with pure efficiency improvements are not possible. However, combined with the described additional measures, it plays an important role to counteract the increasing costs of renewable energy carriers.
- Due to the small database for the prediction of contrails by hydrogen burning turbofan engines, there is a significant uncertainty which will be tackled in future work. Furthermore, the uncertainties for low-NO_x and low-soot combustion of the hydro-carbon powered concepts is rather high, as the effect of reduced soot emissions at contrail impact reduction is not yet understood profoundly.
- The Mach number and altitude constraint variation should be increased in future studies, also including the change in thrust provider from ducted fans to open rotors down to propellers for lower Mach numbers. This could significantly boost the vehicle performance and reduce the climate impact even more.
- Overall, it can be concluded that a significant climate impact reduction in these representative mid-range aircraft is possible with both synthetic kerosene and liquid hydrogen together with advanced combustion chamber technologies and effective contrail avoidance strategies. However, it cannot be concluded which energy carrier has a higher potential for this scenario, as the uncertainties, especially for contrail impact, are rather high.

Author Contributions: Conceptualization, D.S.; methodology, D.S., K.D., A.G., F.L., J.Z., B.R., T.M. and C.J.; software, D.S., K.D., A.G., F.L., J.Z., B.R., T.M. and C.J.; validation, D.S., K.D., A.G., F.L., J.Z., B.R., T.M. and C.J.; formal analysis, D.S., K.D., A.G., F.L., J.Z., B.R., T.M. and C.J.; investigation, D.S., K.D., A.G., F.L., J.Z., B.R., T.M. and C.J.; resources, D.S., K.D., A.G., F.L., J.Z., B.R., T.M. and C.J.; data curation, D.S.; writing—original draft preparation, D.S.; writing—review and editing, D.S., K.D., A.G., F.L., J.Z., B.R. and J.H.; visualization, D.S.; supervision, D.S.; project administration, J.H.; and funding acquisition, J.H. All authors have read and agreed to the published version of the manuscript.

Funding: Authors obtained funding from the DLR-internal project EXACT.

Institutional Review Board Statement: Not applicable.

Informed Consent Statement: Not applicable.

Data Availability Statement: The data presented in this study are available on request from the corresponding author. The data are not publicly available due to the usage of commercial software packages and databases.

Conflicts of Interest: The authors declare no conflict of interest.

Abbreviations

The following abbreviations are used in this manuscript:

AN^2	Turbine loading parameter
ATR	Average Temperature Response
BE	Block Energy
BPR	Bypass Ratio
C_L	High Lift Coefficient
CAPEX	Capital Expenditures
CFRP	Carbon Fibre Reinforced Polymers
CiC	Contrail Induced Cloudiness
CPACS	Common Parametric Aircraft Configuration Schema
DAC	Direct Air Capturing
DOC	Direct Operating Costs
EI	Emission Index
EIS	Entry Into Service
FAR	Fuel-to-Air Ratio
FL	Flight Level
FLOX	Flameless Oxidation
GTlab	Gas Turbine Laboratory
HEFA	Hydroprocessed Esters and Fatty Acids
ISA	International Standard Atmosphere
ICAO	International Civil Aviation Organization
LBO	Lean Blow Off
LH2	Liquid Hydrogen
LHV	Lower Heating Value
LoD	Lift-over-Drag ratio
LTO	Landing and Take-Off cycle
$\dot{m}_{Air}$	Air mass flow
MEM	Manufacturing Empty Mass
MLM	Maximum Landing Mass
MTOM	Maximum Take-Off Mass
nvPM	non volatile particles
OEM	Operating Empty Mass
OPR	Overall Pressure Ratio
p_3	Pressure at combustion chamber entry
PAX	Passengers
PFR	Plug Flow Reactor
PSR	Perfectly Stirred Reactor
PtL	Power to Liquid
R_{FL}	Weighting factor
R	Universal gas constant $R = 8.3143\,\mathrm{J/(Mol\,K)}$
RC	Recurring Costs
RCE	Remote Component Environment
RF	Radiative Forcing
S_D	Air Split
SAC	Schmidt-Appleman Criterion
SAF	Sustainable Aviation Fuel
SL	Sea Level
T_3	Temperature at combustion chamber entry
T_Φ	Equilibrium temperature
$T_{\Phi=1}$	Stoichiometry temperature
T_{FL}	Flame temperature
T_{PZ}	Primary zone temperature
TET	Turbine Entry Temperature
TLARs	Top Level Aircraft Requirements

TO	Take-Off
TOC	Top Of Climb
TOFL	Take-Off Field Lengths
TSEC	Thrust Specific Energy Consumption
TSFC	Thrust Specific Fuel Consumption
V_{psr}	Volume of the perfectly stirred reactor
V_{tot}	Volume of total combustion chamber
vPM	volatile particles
Δpn	Relative change in particle number emissions
η	Overall propulsion efficiency
λ	Air-fuel equivalence ratio

Appendix A

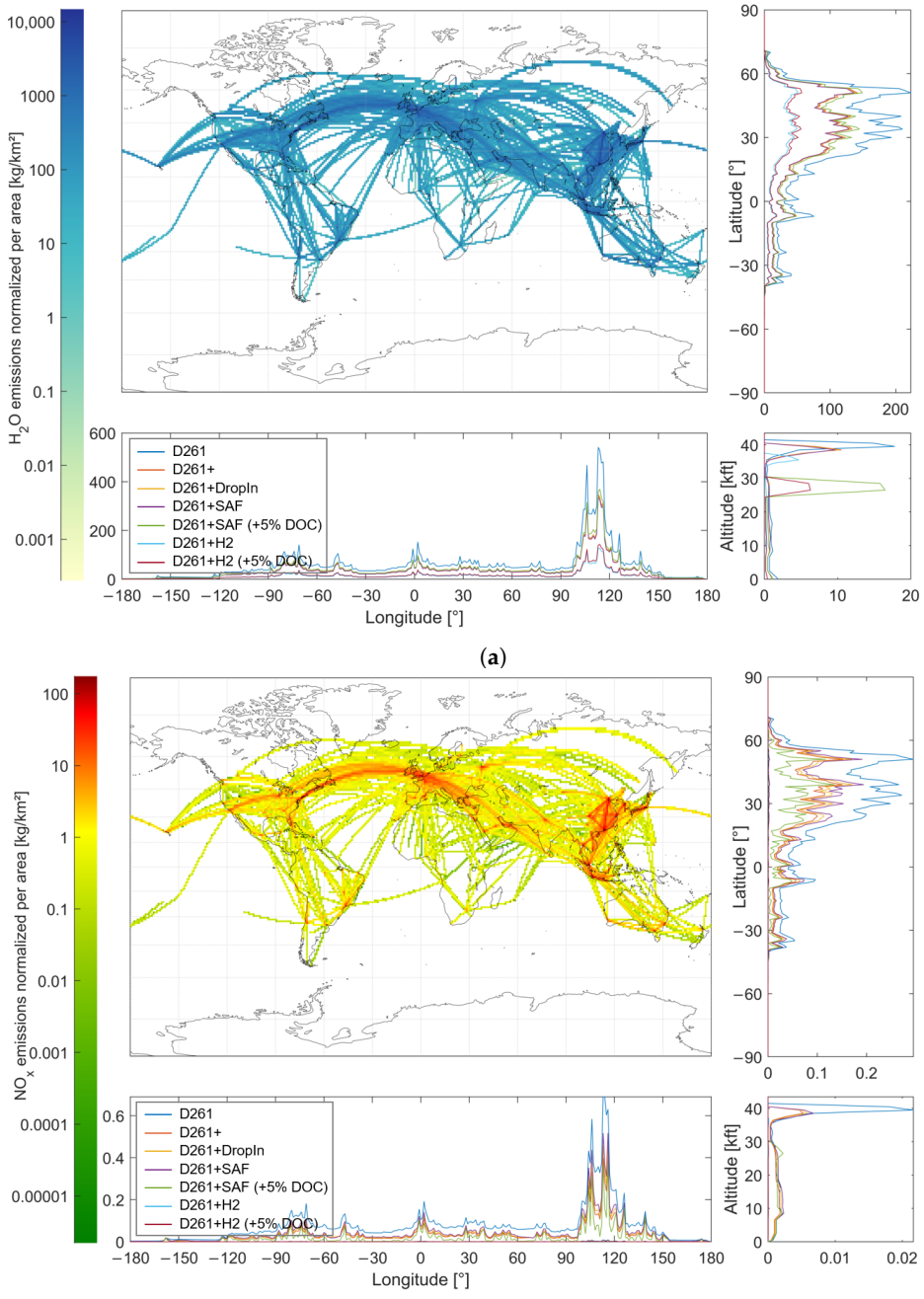

Figure A1. Global distribution of H_2O (**a**) and NO_x (**b**) emissions.

References

1. Voigt, C.; Kleine, J.; Sauer, D.; Moore, R.H.; Bräuer, T.; Le Clercq, P.; Kaufmann, S.; Scheibe, M.; Jurkat-Witschas, T.; Aigner, M.; et al. Cleaner burning aviation fuels can reduce contrail cloudiness. *Commun. Earth Environ.* **2021**, *2*, 114. [CrossRef]
2. Kramer, S.; Andac, G.; Heyne, J.; Ellsworth, J.; Herzig, P.; Lewis, K.C. Perspectives on Fully Synthesized Sustainable Aviation Fuels: Direction and Opportunities. *Front. Energy Res.* **2022**, *9*, 782823. [CrossRef]
3. Goodwin, D.G.; Moffat, H.K.; Speth, R.L. *Cantera: An Object-Oriented Software Toolkit for Chemical Kinetics, Thermodynamics, and Transport Processes*; Caltech: Pasadena, CA, USA, 2009; Volume 124.
4. Chandrasekaran, N.; Guha, A. Study of Prediction Methods for NOx Emission from Turbofan Engines. *J. Propuls. Power* **2012**, *28*, 170–180. [CrossRef]
5. ICAO. *Aircraft Engine Emissions Data Bank*, Version 28; ICAO: Montreal, QC, Canada, 2021.
6. Plohr, M. Anwendungsorientierte Methoden zur Analyse und Modellierung des Emissionsverhaltens Moderner Triebwerke mit Gestuften, Mageren Brennkammersystemen auf Basis Thermodynamischer Triebwerksmodelle. Ph.D. Thesis, Ruhr-Universität Bochum, Universitätsbibliothek, Bochum, Germany, 2016.
7. Stöppler, B. *Entwicklung einer verbesserten Korrelation für die Stickoxidemission von Flugtriebwerken*; Technical Report; Institute of Propulsion Technology, German Aerospace Center (DLR): Berlin, Germany, 1992.
8. Grewe, V.; Stenke, A.; Plohr, M.; Korovkin, V.D. Climate functions for the use in multi-disciplinary optimisation in the pre-design of supersonic business jet. *Aeronaut. J.* **2010**, *114*, 259–269. [CrossRef]
9. Zanger, J.; Monz, T.; Aigner, M. Experimental Investigation of the Combustion Characteristics of a Double-Staged FLOX-Based Combustor on an Atmospheric and a Micro Gas Turbine Test Rig. In Proceedings of the ASME Turbo Expo: Turbine Technical Conference and Exposition—2015, Montreal, QC, Canada, 15–19 June 2015.
10. Seliger-Ost, H.; Kutne, P.; Zanger, J.; Aigner, M. Experimental Investigation of the Impact of Biogas on a 3 kW Micro Gas Turbine FLOX®-Based Combustor. *J. Eng. Gas Turbines Power* **2021**, *143*, 081020. [CrossRef]
11. Hasemann, S.; Huber, A.; Naumann, C.; Aigner, M. Investigation of a FLOX-based Combustor For a Micro gas Turbine With Exhaust Gas Recircuulation. In Proceedings of the ASME Turbo Expo: Turbine Technical Conference and Exposition, Charlotte, NC, USA, 26–30 June 2017.
12. Lingstädt, T.; Grimm, F.; Krummrein, T.; Kutne, P.; Aigner, M. Atmospheric Experimental Investigations of a Jet-Stabilized SOFC Off-Gas Combustor for a Hybrid Power Plant operated with Biogas. In Proceedings of the AIAA Scitech 2019 Forum, San Diego, CA, USA, 7–11 January 2019. [CrossRef]
13. Schwärzle, A.; Monz, T.O.; Huber, A.; Aigner, M. Detailed Examination of a Modified Two-Stage Micro Gas Turbine Combustor. *J. Eng. Gas Turbines Power* **2017**, *140*, 021501. [CrossRef]
14. Zornek, T.; Monz, T.; Aigner, M. Performance analysis of the micro gas turbine Turbec T100 with a new FLOX-combustion system for low calorific fuels. *Appl. Energy* **2015**, *159*, 276–284. [CrossRef]
15. Lammel, O.; Schütz, H.; Schmitz, G.; Lückerath, R.; Stöhr, M.; Noll, B.; Aigner, M.; Hase, M.; Krebs, W. FLOX® Combustion at High Power Density and High Flame Temperatures. *J. Eng. Gas Turbines Power* **2010**, *132*, 121503. [CrossRef]
16. Grimm, F.; Lingstädt, T.; Kutne, P.; Aigner, M. Numerical and Experimental Study of a Jet-and-Recirculation Stabilized Low Calorific Combustor for a Hybrid Power Plant. *Energies* **2021**, *14*, 537. [CrossRef]
17. Lückerath, R.; Meier, W.; Aigner, M. FLOX Combustion at High Pressure With Different Fuel Compositions. *J. Eng. Gas Turbines Power* **2008**, *130*, 011505. [CrossRef]
18. Schmitz, O.; Kaiser, S.; Klingels, H.; Kufner, P.; Obermüller, M.; Henke, M.; Zanger, J.; Grimm, F.; Schuldt, B.; Marcellan, A.; et al. Aero-Engine Concepts Beyond 2030: Part 3—Experimental Demonstration of Technological Feasibility. *ASME. J. Eng. Gas Turbines Power* **2021**, *143*, 021003. [CrossRef]
19. Seliger, H.; Huber, A.; Aigner, M. Experimental Investigation of a FLOX-Based Combustor For a Small-Scale Gas Turbine Based CHP System Under Atmospheric Conditions. In Proceedings of the ASME Turbo Expo: Turbine Technical Conference and Exposition, Montreal, QC, Canada, 15–19 June 2015. [CrossRef]
20. Zanger, J. Experimentelle Charakterisierung eines atmosphärisch betriebenen, jet-stabilisierten Mikrogasturbinenbrenners für Erdgas. Ph.D. Thesis, University of Stuttgart, Stuttgart, Germany, 2016.
21. Kathrotia, T.; Oßwald, P.; Zinsmeister, J.; Methling, T.; Köhler, M. Combustion kinetics of alternative jet fuels, Part-III: Fuel modeling and surrogate strategy. *Fuel* **2021**, *302*, 120737. [CrossRef]
22. Kathrotia, T.; Oßwald, P.; Naumann, C.; Richter, S.; Köhler, M. Combustion kinetics of alternative jet fuels, Part-II: Reaction model for fuel surrogate. *Fuel* **2021**, *302*, 120736. [CrossRef]
23. Glarborg, P.; Miller, J.A.; Ruscic, B.; Klippenstein, S.J. Modeling nitrogen chemistry in combustion. *Prog. Energy Combust. Sci.* **2018**, *67*, 31–68. [CrossRef]
24. ICAO. *Engine Exhaust Emissions Databank*; ICAO: Montreal, QC, Canada, 2021.
25. Reitenbach, S.; Krumme, A.; Behrendt, T.; Schnös, M.; Schmidt, T.; Hönig, S.; Mischke, R.; Mörland, E. Design and application of a multidisciplinary predesign process for novel engine concepts. *J. Eng. Gas Turbines Power* **2019**, *141*, 011017. [CrossRef]
26. Reitenbach, S.; Vieweg, M.; Becker, R.; Hollmann, C.; Wolters, F.; Schmeink, J.; Otten, T.; Siggel, M. Collaborative Aircraft Engine Preliminary Design using a Virtual Engine Platform, Part A: Architecture and Methodology. In Proceedings of the AIAA Scitech 2020 Forum, Orlando, FL, USA, 6–10 January 2020. [CrossRef]

27. Becker, R.G.; Wolters, F.; Nauroz, M.; Otten, T. Development of a gas turbine performance code and its application to preliminary engine design. In Proceedings of the Development of a Gas Turbine Performance Code and Its Application to Preliminary Engine Design, Bremen, Deutschland, 27–29 September 2011.
28. Walsh, P.P.; Fletcher, P. *Gas Turbine Performance*; John Wiley & Sons, Ltd.: Hoboken, NJ, USA, 2004.
29. Grieb, H. *Projektierung von Turboflugtriebwerken*; Springer: Berlin/Heidelberg, Germany, 2013.
30. Guha, A. Optimum fan pressure ratio for bypass engines with separate or mixed exhaust streams. *J. Propuls. Power* **2001**, *17*, 1117–1122. [CrossRef]
31. Vieweg, M.; Reitenbach, S.; Hollmann, C.; Schnös, M.; Behrendt, T.; Krumme, A.; Otten, T.; zu Ummeln, R.M. Collaborative Aircraft Engine Preliminary Design using a Virtual Engine Platform, Part B: Application. In Proceedings of the AIAA Scitech 2020 Forum, Orlando, FL, USA, 6–10 January 2020. [CrossRef]
32. Larsson, L.; Grönstedt, T.; Kyprianidis, K.G. Conceptual design and mission analysis for a geared turbofan and an open rotor configuration. In Proceedings of the ASME 2011 Turbo Expo: Turbine Technical Conference and Exposition, Vancouver, BC, Canada, 6–10 June 2011; Volume 54617, pp. 359–370.
33. German Aerospace Center (DLR). *Simulation and Software Technology, Intelligent and Distributed Systems*; Remote Component Environment; German Aerospace Center: Cologne, Germany, 2020.
34. German Aerospace Center (DLR). *Institute of System Architecture in Aeronautics*; Common Parametric Aircraft Configuration Schema; German Aerospace Center: Cologne, Germany, 2018.
35. Alder, M.; Moerland, E.; Jepsen, J. Recent advances in establishing a common language for aircraft design with CPACS. In Proceedings of the Aerospace Europe Conference, Bordeaux, Frankreich, 25–28 February 2020.
36. Woehler, S.; Atanasov, G.; Silberhorn, D.; Froehler, B.; Zill, T. Preliminary Aircraft Design within a Multidisciplinary and Multi-fidelity Design Environment. In Proceedings of the Aerospace Europe Conference, Bordeaux, Frankreich, 25–28 February 2020.
37. Silberhorn, D.; Arzberger, M.J.; Mennicken, M.; Wolters, F.; Hollmann, C.; Iwanizki, M. Multidisciplinary Investigation of Partially Turboelectric, Boundary Layer Ingesting Aircraft Concepts. In Proceedings of the AIAA Scitech 2020 Forum, Orlando, FL, USA, 6–10 January 2020; p. 0504. [CrossRef]
38. Boeing Commercial Airplanes. *767 Airplane Characteristics for Airport Planning*; D6-58328; Boeing Commercial Airplanes: Seattle, WA, USA, 2021.
39. Burschyk, T.; Cabac, Y.; Silberhorn, D.; Boden, B.; Nagel, B. Liquid hydrogen storage design trades for a short-range aircraft concept. In Proceedings of the Deutscher Luft- und Raumfahrtkongress 2021, Online, 31 August–2 September 2021.
40. Brewer, G.D. *Hydrogen Aircraft Technology*; Routledge: London, UK, 2017. [CrossRef]
41. Hoelzen, J.; Silberhorn, D.; Zill, T.; Bensmann, B.; Hanke-Rauschenbach, R. Hydrogen-powered aviation and its reliance on green hydrogen infrastructure–Review and research gaps. *Int. J. Hydrogen Energy* **2021**, *47*, 3108–3130. [CrossRef]
42. Silberhorn, D.; Hartmann, J.; Dzikus, N.; Atanasov, G.; Zill, T.; Gomez Trillos, J.C.; Oswald, M.; Brand, U.; Vogt, T.; Grimme, W. The Air-Vehicle as a Complex System of Air Transport Energy Systems. In Proceedings of the AIAA Aviation 2020 Forum, Virtual Event, 15–19 June 2020.
43. Thorbeck, J.; Scholz, D. DOC-Assessment Method. In Proceedings of the 3rd Symposium on Collaboration in Aircraft Design, Toulouse, France, 19 September 2013.
44. Thorbeck, J. From Aircraft Performance to Aircraft Assessment. DGLR Short Course: Aircraft Desing. In Proceedings of the Deutsche Gesellschaft für Luft- und Raumfahrt—Lilienthal-Oberth e.V., München, Germany, 5–7 September 2007; pp. 1–56.
45. Beltramo, M.N.; Trapp, D.L.; Kimoto, B.W.; Marsh, D.P. *Parametric Study of Transport Aircraft Systems Cost and Weight*; Science Applications: Los Angeles, CA, USA, 1977.
46. Mottschall, M.; Kasten, P.; Kühnel, S.; Minnich, L. *Sensitivitäten zur Bewertung der Kosten Verschiedener Energieversorgungsoptionen des Verkehrs bis zum Jahr 2050—Abschlussbericht*; Umweltbundesamt, Dessau-Rosslau, Germany, 2019.
47. Grewe, V.; Dahlmann, K.; Flink, J.; Frömming, C.; Ghosh, R.; Gierens, K.; Heller, R.; Hendricks, J.; Jöckel, P.; Kaufmann, S.; et al. Mitigating the Climate Impact from Aviation: Achievements and Results of the DLR WeCare Project. *Aerospace* **2017**, *4*, 34. [CrossRef]
48. Linke, F.; Dahlmann, K.; Gerlinger, B.; Wöhler, S.; Otten, T.; Plohr, M.; Presto, F.; Hartmann, J.; Weiss, M. The impact of a new mid-range aircraft with advanced technologies on air traffic emissions and climate. In Proceedings of the 2020 AIAA AVIATION , Virtual Event, 15–19 June 2020.
49. Linke, F. Environmental Analysis of Operational Air Transportation Concepts (German: Ökologische Analyse Operationeller Lufttransportkonzepte). Ph.D. thesis, Hamburg University of Technology, Hamburg, Germany, 2016.
50. Linke, F.; Grewe, V.; Gollnick, V. The Implications of Intermediate Stop Operations on Aviation Emissions and Climate. *Meteorol. Z.* **2017**, *26*, 697–709. [CrossRef]
51. Grewe, V.; Stenke, A. AirClim: An efficient tool for climate evaluation of aircraft technology. *Atmos. Chem. Phys.* **2008**, *8*, 4621–4639. [CrossRef]
52. Dahlmann, K.; Koch, A.; Linke, F.; Lührs, B.; Grewe, V.; Otten, T.; Seider, D.; Gollnick, V.; Schumann, U. Climate-Compatible Air Transport System—Climate Impact Mitigation Potential for Actual and Future Aircraft. *Aerospace* **2016**, *3*, 38. [CrossRef]
53. Stenke, A.; Grewe, V.; Ponater, M. Lagranian transport of water vapor and cloud water in the ECHAM4 GCM and its impact on the cold bias. *Clim. Dyn.* **2008**, *31*, 491–506. [CrossRef]

54. Burkhardt, U.; Kärcher, B. Process-based simulation of contrail cirrus in a global climate model. *J. Geophys. Res.* **2009**, *114*, D16201. [CrossRef]
55. Hasselmann, K.; Hasselmann, S.; Giering, R.; Ocana, V.; Storch, H.V. Sensitivity Study of Optimal CO_2 Emission Paths Using a Simplified Structural Integrated Assessment Model (SIAM). *Clim. Chang.* **1997**, *37*, 345–386. [CrossRef]
56. Burkhardt, U.; Bock, L.; Bier, A. Mitigating the contrail cirrus climate impact by reducing aircraft soot number emissions. *NPJ Clim. Atmos. Sci.* **2018**, *1*, 37. [CrossRef]
57. Grewe, V.; Gangoli Rao, A.; Grönstedt, T.; Xisto, C.; Linke, F.; Melkert, J.; Middel, J.; Ohlenforst, B.; Blakey, S.; Christie, S.; et al. Evaluating the climate impact of aviation emission scenarios towards the Paris agreement including COVID-19 effects. *Nat. Commun.* **2021**, *12*, 3841. [CrossRef] [PubMed]
58. Gierens, K. Selected topics on the interaction between cirrus clouds and embedded contrails. *Atmos. Chem. Phys.* **2012**, *12*, 11943–11949. [CrossRef]
59. Meinshausen, M.; Smith, S.J.; Calvin, K.; Daniel, J.S.; Kainuma, M.L.T.; Lamarque, J.F.; Matsumoto, K.; Montzka, S.A.; Raper, S.C.B.; Riahi, K.; et al. The RCP greenhouse gas concentrations and their extensions from 1765 to 2300. *Clim. Chang.* **2011**, *109*, 213–241. [CrossRef]
60. Zanger, J.; Monz, T.; Aigner, M. Experimental Investigation of the Influence of Combustor Cooling on the Characteristics of a FLOX-Based Micro Gas Turbine Combustor. In *Progress in Gas Turbine Performance*; Benini, E., Ed.; InTech: Lodon, UK, 2013; ISBN 978-953-51-1166-5, pp. 165–184.
61. European Union Aviation Safety Agency. *Certification Specifications and Acceptable Means of Compliance for Large Aeroplanes CS-25, Amendment 26*; European Union Aviation Safety Agency: Cologne, Germany, 2020.